Optics Letters

Simultaneous two-photon resonant optical laser locking (STROLLing) in the hyperfine Paschen–Back regime

RENJU S. MATHEW,* [ID] FRANCISCO PONCIANO-OJEDA, [ID] JAMES KEAVENEY, DANIEL J. WHITING, AND IFAN G. HUGHES

Department of Physics, Joint Quantum Centre (JQC) Durham-Newcastle, Durham University, South Road, Durham DH1 3LE, UK
Corresponding author: r.s.mathew@durham.ac.uk

We demonstrate a technique to lock simultaneously two laser frequencies to each step of a two-photon transition in the presence of a magnetic field sufficiently large to gain access to the hyperfine Paschen–Back regime. A ladder configuration with the $5S_{1/2}$, $5P_{3/2}$, and $5D_{5/2}$ terms in a thermal vapor of ^{87}Rb atoms is used. The two lasers remain locked for more than 24 h. For the sum of the laser frequencies, which represents the stability of the two-photon lock, we measure a frequency instability of less than the Rb D_2 natural linewidth of 6 MHz for nearly all measured timescales.

https://doi.org/10.1364/OL.43.004204

Stabilizing the optical output frequency of a laser, commonly known as laser locking, is essential for many areas of research. This is particularly true in atomic physics where the required absolute stability, being dictated by the width of atomic resonance lines, can often be sub-megahertz. A plethora of methods have been developed for on- or near-resonant locking. Recent interest in performing thermal vapor experiments in the hyperfine Paschen–Back (HPB) regime [1–9], where the atomic resonances are typically Zeeman-shifted by tens of gigahertz, necessitates new methods of laser locking. In this Letter, we demonstrate a novel method for laser locking to a Zeeman-shifted two-photon transition.

The currently available methods for on- or near-resonant locking include locking to stable optical cavities [10], wavelength meters [11], and beat-note locks [12,13]. In atomic physics research, lasers are often stabilized to a particular atomic resonance line. A variety of spectroscopic techniques can be used to generate a dispersive error signal with a zero crossing at the lock point. These include frequency modulation [14] and modulation transfer spectroscopy [15,16], which require external modulation of the laser to generate the dispersive lock

signals. Other methods such as polarization spectroscopy [17], saturated absorption spectroscopy [18], dichroic atomic vapor laser locking [19–22], and prismatic deflection [23] do not require external modulation and, therefore, are experimentally simpler to implement. The Faraday effect can also be exploited to form an off-resonance laser lock [24], as can Zeeman-shift based locking [25], both of which have the advantage of being tunable over a relatively wide range. The laser frequency can also be stabilized at large detunings using saturation absorption spectroscopy [26] and a low-quality cavity technique [27].

Alternatively, lasers can be intrinsically stabilized by placing atomic media in the external cavity feedback, obviating the need for external locking [28]. In multi-level atomic systems coupled with several lasers, the excited-state transitions can also be used as locking signals with some variations on the techniques above. These include locks based on electromagnetically induced transparency (EIT) [29–31], fluorescence detection [32], and excited-state polarization spectroscopy with [33] and without [34] a small magnetic field. As our experiments are done in the HPB regime, none of the aforementioned techniques is immediately suitable for our purposes. Furthermore, quantum optics experiments [35–40] often require long integration times [41], meaning that lasers may need to remain locked for several hours.

Here we present a technique to lock simultaneously two lasers to two transitions that form a ladder-type excitation scheme (see Fig. 1), thus stabilizing the sum of their frequencies over a timescale of hours in a thermal vapor of ^{87}Rb in the presence of a large magnetic field (0.6 T). This field is large enough to gain access to the HPB regime and for the Zeeman shift to exceed the Doppler width. Both transitions are significantly Zeeman-shifted from their zero-field frequencies. Beyond being able to work in large fields, other advantages of our scheme include tunability on the first step of the excitation and the lock compensating for drift in one laser by automatic adjustment of the other.

We first use the off-resonant Faraday rotation method described in Ref. [24] to stabilize the 780 nm probe laser and then use a novel Faraday EIT method to stabilize the 776 nm coupling laser. In order to create a suitable crossing
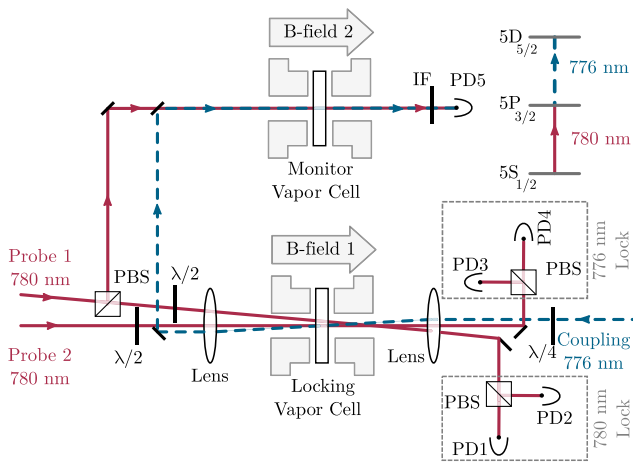
Fig. 1. Schematic of the experimental configuration. The probe beams (red solid lines) and coupling beam (blue dashed line) are counterpropagated and focused through the locking vapor cell with a path length of 1 mm containing isotopically enriched ^{87}Rb in a uniform magnetic field of up to 0.6 T along the beam axis. Only probe beam 2 and the coupling beam are overlapped within the cell. The angles are not to scale. The beam polarizations are set by a half- and quarter-wave plates ($\lambda/2$ & $\lambda/4$). The Stokes parameter S_1 is measured by subtracting the signals from the photodiodes (PDs) at the output of a PBS. PDs 1 and 2 are for the 780 nm lock, and 3 and 4 are for the 776 lock. The atomic resonance of interest is monitored using the monitor vapor cell, interference filter (IF) and PD5. The rubidium energy levels used are indicated on the top right.

for the resonances of interest to us, our simultaneous two-photon resonant optical laser lock (STROLL) is implemented in the HPB regime.

Measurement of the optical rotation due to the Faraday effect near an atomic resonance provides an error signal to which the probe laser can be locked [24]. For an atomic medium in an external axial magnetic field, there are different refractive indices for right- and left-handed circularly polarized light (circular birefringence). This leads to the rotation of the plane of polarization of linearly polarized input light, where the rotation angle is proportional to the real part of the difference in refractive indices. The degree of rotation depends on the detuning of the light from the atomic resonances allowing the laser to be stabilized. The rotation is measured using the Stokes parameter, $S_1 = (I_x - I_y)/I_0$, which is the normalized difference in the intensities of orthogonal linear polarization components of the output light (see Fig. 1). The denominator I_0, the incident intensity, normalizes the definition so that S_1 lies between -1 and 1 and so the line shape of S_1 has a zero crossing. As shown on the bottom panel of Fig. 2(b), we can use an appropriate zero crossing in S_1 as an error signal to the feedback loop of our probe laser PID (proportional-integral-derivative) controller.

With the 780 nm probe laser locked, we can now lock the 776 nm coupling beam. We use a second probe beam that is overlapped with the coupling beam in the locking cell, while ensuring that the first probe beam is not overlapped with the coupling beam. This configuration of beams leads to the presence of an EIT feature. EIT is a well-used technique in multi-level atomic systems [46,47]. It describes the reduction in the absorption of a weak probe laser when a strong coupling laser field is used to drive a resonant transition in a three-level atomic

system, where the two resonant transitions are coherently coupled to a common state. Associated with the change in absorption, EIT results in a concomitant modification of the refractive index [48]. In the HPB regime, the EIT feature only couples to one transition and, thus, only changes the refractive index of one hand of polarization—hence, EIT causes additional birefringence and a change in the S_1 signal [24]. EIT appears as a dispersive feature on the S_1 signal when the probe laser is scanning, and the coupling beam is on and at a fixed frequency [see Fig. 2(c), highlighted region]. When the probe laser is locked and the coupling beam is scanning, we use this feature as the error signal [see Fig. 2(d)] to the PID feedback loop of our coupling laser controller.

Figure 1 shows a schematic of the experimental setup. Two weak (50 μW) probe beams are focused to a beam ellipse with waists of 83 ± 2 μm × 106 ± 2 μm (measured using [49]) through a 1 mm long heated vapor cell (the "locking vapor cell") of isotopically enriched rubidium (> 98%^{87}Rb). A strong (16 mW) 776 nm coupling beam is focused to a beam ellipse with waists of 74 ± 2 μm × 80 ± 2 μm [49] and counterpropagated through the cell. The second probe beam and the coupling beam, which are resonant with the $|5S_{1/2}, m_J = \frac{1}{2}\rangle \rightarrow |5P_{3/2}, m_J = \frac{3}{2}\rangle$ and $|5P_{3/2}, m_J = \frac{3}{2}\rangle \rightarrow |5D_{5/2}, m_J = \frac{1}{2}\rangle$ transitions respectively, are overlapped within the same cell. We note that an advantage of our scheme is that most of the strong coupling beam can be reused in further experiments. The raw intensity differences (i.e., $I_x - I_y$) are generated with the use of polarizing beam splitters (PBSs) and photodiodes (PD1 and PD2 for the probe lock, and PD3 and PD4 for the coupling lock).

The probe and coupling light are also sent through a 2 mm long heated vapor cell (the "monitor vapor cell") of isotopically enriched rubidium (> 98%^{87}Rb). Monitoring the absorption in this cell using a photodiode (PD5) allows choice over where to lock the 780 nm laser. This can be seen in Fig. 2(a), where the zero crossing on the bottom panel is chosen depending on which resonance from the top panel is of interest. Both cells contain unknown buffer gas which causes an additional broadening of 7 MHz on the D_2 line.

Across each vapor cell, two cylindrical NdFeB magnets—Fig. 1 shows a cross-sectional view of the top-hat profile of the magnets—are used to achieve a magnetic field of up to 0.6 T. The strength of each field can be varied by changing the separation of the respective magnets. By changing the strength of the field across the locking cell, we have tunability for the lock point of the 780 nm laser, although the STROLL will remain locked to the two-photon resonance. The field over the region occupied by the 2 mm vapor cell has an rms variation of 4 μT. Further details of field uniformity and magnet design can be found in Refs. [50,51].

To monitor the long-term stability of the locked lasers, Fig. 3 shows the overlapping Allan deviation [52,53] of the concurrent frequency measurement of the 776 and 780 nm diode lasers, where we have used a high finesse WS7 wavemeter with a switcher box to simultaneously monitor both laser frequencies over a period of 24 h. The lasers remain locked for the whole period. When locked, the frequency instability of the sum of both lasers is less than the natural linewidth of the probe transition of 6 MHz and of the EIT linewidth of 25 MHz. It is clear that, for most timescales, the frequency instability of the sum is less than the frequency instability of either the 780 or 776 nm laser. STROLL keeps the lasers
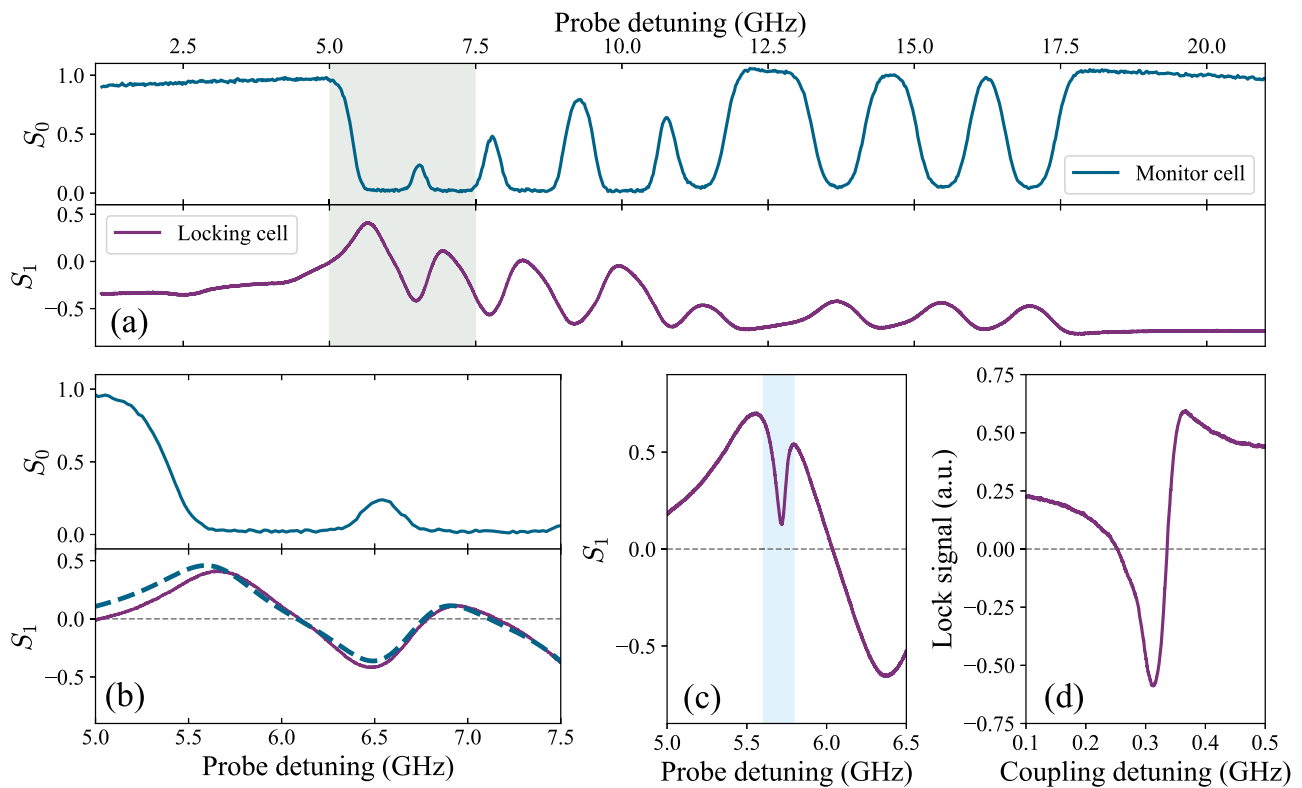
Fig. 2. (a) Monitor cell spectrum (top) is used to locate the required zero crossing on the locking cell signal (bottom). With only probe beam 1 on, the top panel shows the 780 nm spectrum in the hyperfine Paschen–Back regime in the monitor cell at 106°C, and the bottom panel shows the S_1 signal in the locking cell at 100°C. This temperature is a compromise between the increased signal and the optical depth and line broadening. Zero probe detuning is the weighted D_2 line center of naturally abundant rubidium in a zero magnetic field [42]. (b) S_1 signal from probe beam 1 has a zero crossing that can be used in (d) to lock the probe laser. Shown is the shaded region from (a) where the dashed line is an ElecSus fit [43–45]. (c) S_1 signal from probe beam 2 has an EIT feature (shaded region) when the coupling beam is turned on and resonant. (d) With the probe laser now locked [using the method shown in part (b)], scanning the coupling laser gives the error signal used to lock the coupling laser.

locked to the two-photon transition: although the frequency of one laser may drift, the frequency of the other changes accordingly to compensate. When unlocked, the lasers stay at an equivalent stability only for averaging times less than 15 min. This becomes important for quantum optics measurements where data must be accumulated over hours [8], e.g., $g^{(2)}$ autocorrelation measurements.

Further improvements to the stability could be achieved, if desired, by adding active temperature stabilization. In this Letter, the cell temperature was measured to be stable to better than 1°C over several hours; this measurement also revealed that the peaks at 150 s in Fig. 3 are almost certainly due to temperature variation. The laser frequency stability achieved is sufficient for our purposes. However, temperature sensitivity is a known issue with Faraday locking [24], with a temperature dependence of the zero crossing of <1 MHz/°C.

The tunability of the probe laser lock point is set by the strength of the magnetic field which gives several gigahertz of freedom. Further freedom arises from the presence of many possible zero crossings in the S_1 signal (because the Zeeman shift exceeds the Doppler width), as is seen in Fig. 2(a) and from our PID electronics allowing us to choose different setpoint voltages.

We have demonstrated a technique to lock simultaneously two laser frequencies to the two-photon transition, $5S_{1/2} \rightarrow 5D_{5/2}$ in ^{87}Rb in the presence of an applied magnetic field
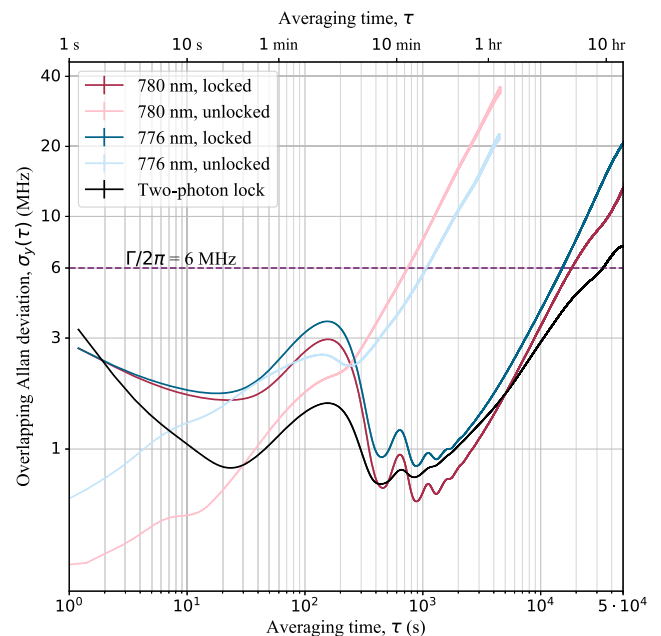

Fig. 3. Overlapping Allan deviation of the frequency measurement of the 780 nm probe laser, the 776 nm coupling laser, and the summed frequency. Γ is the natural linewidth of the $5S \rightarrow 5P$ probe transition.

that is large enough to gain entry to the HPB regime. When locked simultaneously, we showed a frequency instability for the sum frequency of less than 6 MHz for nearly all measured timescales. While in this Letter the specific application was in rubidium, the concept is easily transferrable to three-level ladder systems in other alkali metals.

REFERENCES

1. B. A. Olsen, B. Patton, Y.-Y. Jau, and W. Happer, Phys. Rev. A **84**, 63410 (2011).
2. A. Sargsyan, G. Hakhumyan, C. Leroy, Y. Pashayan-Leroy, A. Papoyan, D. Sarkisyan, and M. Auzinsh, J. Opt. Soc. Am. B **31**, 1046 (2014).
3. A. Sargsyan, A. Tonoyan, G. Hakhumyan, C. Leroy, Y. Pashayan-Leroy, and D. Sarkisyan, Europhys. Lett. **110**, 23001 (2015).
4. A. Sargsyan, A. Tonoyan, G. Hakhumyan, C. Leroy, Y. Pashayan-Leroy, and D. Sarkisyan, Opt. Commun. **334**, 208 (2015).
5. A. Sargsyan, E. Klinger, A. Tonoyan, C. Leroy, and D. Sarkisyan, J. Phys. B **51**, 145001 (2018).
6. D. J. Whiting, E. Bimbard, J. Keaveney, M. A. Zentile, C. S. Adams, and I. G. Hughes, Opt. Lett. **40**, 4289 (2015).
7. D. J. Whiting, J. Keaveney, C. S. Adams, and I. G. Hughes, Phys. Rev. A **93**, 43854 (2016).
8. D. J. Whiting, N. Šibalić, J. Keaveney, C. S. Adams, and I. G. Hughes, Phys. Rev. Lett. **118**, 253601 (2017).
9. D. J. Whiting, R. S. Mathew, J. Keaveney, C. S. Adams, and I. G. Hughes, J. Mod. Opt. **65**, 713 (2018).
10. R. W. P. Drever, J. L. Hall, F. V. Kowalski, J. Hough, G. M. Ford, A. J. Munley, and H. Ward, Appl. Phys. B **31**, 97 (1983).
11. S. Kobtsev, S. Kandrushin, and A. Potekhin, Appl. Opt. **46**, 5840 (2007).
12. T. Day, E. K. Gustafson, and R. L. Byer, IEEE J. Quantum Electron. **28**, 1106 (1992).
13. T. Uehara, K. Tsuji, K. Hagiwara, and N. Onodera, Opt. Eng. **53**, 124109 (2014).
14. G. C. Bjorklund, Opt. Lett. **5**, 15 (1980).
15. J. H. Shirley, Opt. Lett. **7**, 537 (1982).
16. D. J. McCarron, S. A. King, and S. L. Cornish, Meas. Sci. Technol. **19**, 105601 (2008).
17. C. P. Pearman, C. S. Adams, S. G. Cox, P. F. Griffin, D. A. Smith, and I. G. Hughes, J. Phys. B **35**, 5141 (2002).
18. G. R. Hanes and C. E. Dahlstrom, Appl. Phys. Lett. **14**, 362 (1969).
19. K. L. Corwin, Z. T. Lu, C. F. Hand, R. J. Epstein, and C. E. Wieman, Appl. Opt. **37**, 3295 (1998).
20. T. Petelski, M. Fattori, G. Lamporesi, J. Stuhler, and G. M. Tino, Eur. Phys. J. D **22**, 279 (2003).
21. M. L. Harris, S. L. Cornish, A. Tripathi, and I. G. Hughes, J. Phys. B **41**, 085401 (2008).
22. F. E. Becerra, R. T. Willis, S. L. Rolston, and L. A. Orozco, J. Opt. Soc. Am. B **26**, 1315 (2009).
23. G. T. Purves, G. Jundt, C. S. Adams, and I. G. Hughes, Eur. Phys. J. D **29**, 433 (2004).
24. M. A. Zentile, R. Andrews, L. Weller, S. Knappe, C. S. Adams, and I. G. Hughes, J. Phys. B **47**, 75005 (2014).
25. D. J. Reed, N. Šibalić, D. J. Whiting, J. M. Kondo, C. S. Adams, and K. J. Weatherill, "Low-drift Zeeman shifted atomic frequency reference," arXiv: 1804.07928 (2018).
26. A. Sargsyan, A. Tonoyan, R. Mirzoyan, D. Sarkisyan, A. M. Wojciechowski, A. Stabrawa, and W. Gawlik, Opt. Lett. **39**, 2270 (2014).
27. P. M. T. Barboza, G. G. Nascimento, M. O. Araújo, C. M. da Silva, H. L. D. d. S. Cavalcante, M. Oriá, M. Chevrollier, and T. P. de Silans, J. Phys. B **49**, 085401 (2016).
28. J. Keaveney, W. J. Hamlyn, C. S. Adams, and I. G. Hughes, Rev. Sci. Instrum. **87**, 95111 (2016).
29. R. P. Abel, A. K. Mohapatra, M. G. Bason, J. D. Pritchard, K. J. Weatherill, U. Raitzsch, and C. S. Adams, Appl. Phys. Lett. **94**, 71107 (2009).
30. S. C. Bell, D. M. Heywood, J. D. White, J. D. Close, and R. E. Scholten, Appl. Phys. Lett. **90**, 171120 (2007).
31. A. Sargsyan, A. V. Papoyan, D. Sarkisyan, and A. Weis, Eur. Phys. J. Appl. Phys. **48**, 20701 (2009).
32. A. Y. Kalatskiy, A. E. Afanasiev, P. N. Melentiev, and V. I. Balykin, Laser Phys. **27**, 055703 (2017).
33. M. Parniak, A. Leszczyński, and W. Wasilewski, Appl. Phys. Lett. **108**, 161103 (2016).
34. C. Carr, C. S. Adams, and K. J. Weatherill, Opt. Lett. **37**, 118 (2012).
35. H.-R. Noh and H. S. Moon, Opt. Express **19**, 11128 (2011).
36. H.-R. Noh and H. S. Moon, Phys. Rev. A **92**, 013807 (2015).
37. Y.-S. Lee, S. M. Lee, H. Kim, and H. S. Moon, Opt. Express **24**, 28083 (2016).
38. Y.-S. Lee, S. M. Lee, H. Kim, and H. S. Moon, Phys. Rev. A **96**, 63832 (2017).
39. B. Srivathsan, G. K. Gulati, B. Chng, G. Maslennikov, D. Matsukevich, and C. Kurtsiefer, Phys. Rev. Lett. **111**, 123602 (2013).
40. B. Huber, A. Kölle, and T. Pfau, Phys. Rev. A **90**, 53806 (2014).
41. R. T. Willis, F. E. Becerra, L. A. Orozco, and S. L. Rolston, Opt. Express **19**, 14632 (2011).
42. P. Siddons, C. S. Adams, C. Ge, and I. G. Hughes, J. Phys. B **41**, 155004 (2008).
43. M. A. Zentile, J. Keaveney, L. Weller, D. J. Whiting, C. S. Adams, and I. G. Hughes, Comput. Phys. Commun. **189**, 162 (2015).
44. J. Keaveney, C. S. Adams, and I. G. Hughes, Comput. Phys. Commun. **224**, 311 (2017).
45. I. G. Hughes and T. P. A. Hase, *Measurements and Their Uncertainties: A Practical Guide to Modern Error Analysis* (Oxford University, 2010).
46. M. Fleischhauer, A. Imamoglu, and J. P. Marangos, Rev. Mod. Phys. **77**, 633 (2005).
47. H. S. Moon and H.-R. Noh, Phys. Rev. A **84**, 033821 (2011).
48. D. Budker, D. Kimball, S. Rochester, and V. Yashchuk, Phys. Rev. Lett. **83**, 1767 (1999).
49. J. Keaveney, Rev. Sci. Instrum. **89**, 035114 (2018).
50. D. J. Whiting, "Nonlinear optics in a thermal Rb vapour at high magnetic fields," Ph.D. dissertation (Durham University, 2017).
51. M. A. Zentile, "Applications of the Faraday effect in hot atomic vapours," Ph.D. dissertation (Durham University, 2015).
52. W. J. Riley and D. A. Howe, "Handbook of frequency stability analysis," Report No. 1065, Special Publications (NIST SP) (NIST, 2008).
53. D. Allan, Proc. IEEE **54**, 221 (1966).